Time domain prediction of first- and second-order wave forces on rigid and elastic floating bodies

KARA, Fuat

Citation:

Copyright and re-use policy

Time domain prediction of first- and second-order wave forces on rigid and elastic floating bodies

Fuat Kara

Sheffield Hallam University, UK, S1 1WB, fuat.kara@shu.ac.uk

Abstract

The application and development of a transient three-dimensional numerical code ITU-WAVE which is based on panel method, potential theory and Neumann-Kelvin linearization is presented for the prediction of hydrodynamics characteristics of mono-hull and multi-hull floating bodies. The time histories of unsteady motions in ambient incident waves are directly presented with regards to impulse response functions (IRFs) in time. The first order steady forces of wave-resistance, sinkage force and trim moment are solved as the steady state limit of surge radiation IRFs. The numerical prediction of the second order mean force which can be computed from quadratic product of first-order quantities is presented using near-field method based on the direct pressure integration over floating body in time domain. The hydrodynamic and structural parts are fully coupled through modal analysis for the solution of hydroelastic problem in which Euler-Bernoulli beam is used for the structural analysis. A stiff structure is then studied assuming that contributions of rigid body modes are much bigger than elastic modes. A discrete control of latching is used to increase the bandwidth of the efficiency of Wave Energy Converters (WEC). ITU-WAVE numerical results for different floating bodies show acceptable agreements compared to analytical, other numerical and experimental results.

Keywords: seakeeping, mono- and multi-hull floating bodies, the first and second order steady forces, hydroelasticity, wave energy converters, time domain, transient free-surface wave Green function, boundary integral equation method

1. Introduction

The prediction of the local and global responses of floating bodies to excitation by waves is the fundamental problem involving a three dimensional rigid and elastic mono- and multi-hull structures, either moving with forward speed or stationary at the interface of two fluids and introducing interactions between the fluid and structures. The flow field around a body and the resulting motion due to incident waves requires a three dimensional non-linear analysis for accurate predictions of hydrodynamic parameters. The complete solution of this kind of problem may be obtained by solving Navier-Stokes equations using computational fluid dynamics methods. Another approach for the non-linear analysis is the use of a viscous solution in the near field and an inviscid solution in the far field. However, the required computational time to solve these kinds of problems is not suitable for practical purposes.

An alternative approach to a viscous solution is the potential flow formulation to solve the hydrodynamic problem. The application of potential flow approximation in two-dimensions was used as a basis to develop the strip theory (Korvin-Kroukovsky 1957, Ogilvie *et.al.* 1969, Salvensen *et.al.* 1970 and Kim *et.al* 1980). Because of the computational simplicity and the satisfactory approximation of the body motion of conventional ships, strip theory is still in use to date. However, for the low frequency, high forward speed case and complex body shapes, the prediction of global loads based on strip theory gives inaccurate results.

As the hydrodynamic interactions are inherently three-dimensional, three-dimensional numerical approximations need to be used for accurate prediction of the wave loads and motions. As each discretized panel would have its influence on all other panels, the hydrodynamic interactions effects are automatically taken into account in three-dimensional numerical models. The prediction of three-dimensional effects can be obtained using three-dimensional frequency and time domain approaches and two popular approaches were used for this purpose. These are Green's function approximation (Liapis and Beck 1985, Liapis 1986, King 1987, Lin and Yue 1990, Kara 2000, Inoue 2008) or Rankine type source distribution (Betram 1990,

Nakos et.al. 1990, Kring and Sclavonous 1991, Xiang and Faltinsen 2011, Yuan et.al. 2014). The former satisfies the free surface boundary condition and condition at infinity automatically, and only the body surface needs to be discretized with panels, while in the latter source and dipole singularities are distributed discretizing both the body surface and a portion of the free surface. The main disadvantage of Rankine type source distribution is the stability problem for the numerical implementation, since the radiation condition or condition at infinity is not satisfied exactly. The requirement of the discretization of some portion of the free surface using quadrilateral or triangular elements increases the computational time. The time domain and frequency domain results are related by the Fourier transform in the context of the linear theory.

The prediction of the unsteady non-linear body motions can be obtained by the use of the semi non-linear approaches (Ferrant 1990, Beck *et.al*. 1991 and Lin *et.al*. 1990, Danmeier 1999). In the semi non-linear approach, the interactions between steady and unsteady problems are coupled. The free surface boundary condition is linearized, which results in the use of the transient free surface Green function in the *body exact* method, while the body boundary condition is satisfied on the instantaneous body surface, which results in a time varying system. In this case, time and frequency domain solutions are not related by the use of Fourier transform. The resultant hydrodynamic forces over the body surface, in the case of the Neumann-Kelvin linearization, gives rise to sinusoidal excitation, while the hydrodynamic forces over the body surface using the body exact boundary condition are not sinusoidal. The evaluation of the convolution integrals, which requires the recalculation of the transient free surface Green function at each time step, increases the computational time significantly in the case of constant panel method.

In the context of potential approximation, the fully non-linear body motion of floating bodies can be predicted using the mixed Euler-Lagrange method (Longuet-Higgins 1976, Faltinsen 1977, Baker *et.al*. 1982, Vinje *et.al*. 1981 and Beck 1999) which has two steps: Lagrangean and Eulerian. The fluid velocities used to integrate the free surface boundary conditions are obtained in the Eulerian step solving the linear boundary value problem. The integration of the non-linear free surface boundary conditions in terms of time are evaluated in the Lagrangean step.

The extension of the time domain approach to more general cases, such as non-constant forward speed case, large amplitude body motion, water on deck, unsteady manoeuvres of the body surface, non-linear cable forces, determine the first order steady forces (e.g. wave making resistance, sinkage force and trim moment) as a large-time limit, inclusion of semi-empirical non-linear roll damping, non-linear hydrostatic effects, transient behaviour of wave induced hydroelasticity of floating bodies etc., is much easier than the frequency domain approach.

In the present paper, the fluid boundaries are described by the use of Boundary Integral Equation Method (BIEM) with Neumann-Kelvin linearization. The exact initial boundary value problem is then linearized using the free stream as a basis flow and replaced by the boundary integral equation applying Green theorem over three-dimensional transient free surface Green function (Kara and Kara et.al. 2000-2017). The resultant boundary integral equation is discretized using quadrilateral panels over which the value of the potential is assumed to be constant and solved using the trapezoidal rule to integrate the memory part of the transient free surface Green function in time. The free surface and body boundary conditions are linearized on the discretized collocation points over each quadrilateral element to obtain algebraic equation. The accuracy of ITU-WAVE computational numerical results is assessed by comparing with the available analytical, other numerical and experimental results.

2. Theory - solution of boundary integral equation

The initial boundary value problem consisting of initial, free surface and body boundary conditions for the solution may be represented as an integral equation using a transient free surface Green's function (Wehausen and Laitone 1960). This integral equation is derived by applying Green's theorem over the transient free surface Green function which satisfies the initial boundary value problem without a body

(Finkelstein 1957). Integrating Green's theorem in terms of time from $-\infty$ to $+\infty$ using the properties of transient free surface Green's function and potential theory, the integral equation for the potential approximation on the body surface may be written as (Kara 2000).

$$\varphi(P,t) + \frac{1}{2\pi} \iint\limits_{S_{b(t)}} dS_Q\, \varphi(Q,t) \frac{\partial}{\partial n_Q}\left(\frac{1}{r} - \frac{1}{r'}\right) = \frac{1}{2\pi} \iint\limits_{S_{b(t)}} dS_Q\left(\frac{1}{r} - \frac{1}{r'}\right)\frac{\partial}{\partial n_Q}\varphi(Q,t)$$

$$-\frac{1}{2\pi}\int_{t_0}^{t} d\tau \iint\limits_{S_{b(\tau)}} dS_Q\left\{\varphi(Q,\tau)\frac{\partial}{\partial n_Q}\tilde{G}(P,Q,t-\tau) - \tilde{G}(P,Q,t-\tau)\frac{\partial}{\partial n_Q}\varphi(Q,\tau)\right\}$$

$$-\frac{U_0^2}{2\pi g}\int_{t_0}^{t} d\tau \oint_{\Gamma(\tau)} d\eta\left\{\varphi(Q,\tau)\frac{\partial}{\partial \xi}\tilde{G}(P,Q,t-\tau) - \tilde{G}(P,Q,t-\tau)\frac{\partial}{\partial \xi}\varphi(Q,\tau)\right\}$$

$$-\frac{U_0}{2\pi g}\int_{t_0}^{t} d\tau \oint_{\Gamma(\tau)} d\eta\left\{\varphi(Q,\tau)\frac{\partial}{\partial \tau}\tilde{G}(P,Q,t-\tau) - \tilde{G}(P,Q,t-\tau)\frac{\partial}{\partial \tau}\varphi(Q,\tau)\right\}$$

(1)

If the fluid velocities are required on the body surface directly, it is more convenient to use source formulation as fluid velocities can be obtained directly whilst potential approximation Eq. (1) requires the first order spatial derivatives. Using potential theory, the integral equation for the source strength on the body surface may be written as

$$\frac{1}{2}\sigma(P,t) + \frac{1}{4\pi} \iint\limits_{S_{b(t)}} dS_Q\frac{\partial}{\partial n_P}\left(\frac{1}{r} - \frac{1}{r'}\right)\sigma(Q,t) = -\frac{\partial}{\partial n_P}\varphi(P,t)$$

$$-\frac{1}{4\pi}\int_{t_0}^{t} d\tau \iint_{S_{b(\tau)}} dS_Q\frac{\partial}{\partial n_P}\tilde{G}(P,Q,t-\tau)\sigma(Q,\tau) - \frac{U_0^2}{4\pi g}\int_{t_0}^{t} d\tau \oint_{\Gamma(\tau)} d\eta\, n_1\frac{\partial}{\partial n_P}\tilde{G}(P,Q,t-\tau)\sigma(Q,\tau)$$

(2)

and potential on the body surface

$$\varphi(P,t) = -\frac{1}{4\pi} \iint\limits_{S_{b(t)}} dS_Q\left(\frac{1}{r} - \frac{1}{r'}\right)\sigma(Q,t) - \frac{1}{4\pi}\int_{t_0}^{t} d\tau \iint\limits_{S_{b(\tau)}} dS_Q\tilde{G}(P,Q,t-\tau)\sigma(Q,\tau) - \frac{U_0^2}{4\pi g}\int_{t_0}^{t} d\tau \oint_{\Gamma(\tau)} d\eta n_1 \tilde{G}(P,Q,t-\tau)\sigma(Q,\tau)$$

(3)

where

$$\tilde{G}(P,Q,t,\tau) = 2\int_0^{\infty} dk\sqrt{kg}\sin\left(\sqrt{kg}(t-\tau)\right)e^{k(z+\varsigma)}J_0(kR)$$

$$R = \sqrt{(x-\xi+U_0t)^2 + (y-\eta)^2}$$

$$r = \sqrt{(x-\xi)^2 + (y-\eta)^2 + (z-\varsigma)^2}$$

$$r' = \sqrt{(x-\xi)^2 + (y-\eta)^2 + (z+\varsigma)^2}$$

where $\Gamma(t)$ is the intersection between the body surface and the free surface, $\tilde{G}(P,Q,t,\tau)$ the memory part of the transient free surface Green function, $P(x(t),y(t),z(t))$ the field point, $Q(\xi(t),\eta(t),\varsigma(t))$ the source point, r the distance between field and source point and represent the Rankine part of source potential, r' the distance between field point and image point over free surface, J_0 the Bessel function of zero order. The Green function $\tilde{G}(P,Q,t,\tau)$ represents the potential at the field point $P(x(t),y(t),z(t))$ and time t due to an impulsive disturbance at source point $Q(\xi(t),\eta(t),\varsigma(t))$ and time τ.

The integral equation for the potential Eq. (1) is solved to get the potential directly. In the case of source formulation, the integral equation for the source strength Eq. (2) is first solved, and then this source strength is used in the potential formulation Eq. (3) to find potential and fluid velocities (which are gradient of Eq.(2)) at any point in the fluid domain. The solution of the integral equations Eq. (1) and Eq. (2) is done using time marching scheme. The form of the equation Eq. (1) and Eq. (2) is the same for both the radiation and the diffraction potentials so that the same approach may be used for all potentials. Since the transient free surface Green function $\tilde{G}(P,Q,t,\tau)$ satisfies free surface boundary condition and condition at infinity automatically, in this case only the underwater surface of the body needs to be discretized with panels. The

resultant boundary integral equation Eq. (1) and Eq. (2) in the present paper is discretized using quadrilateral elements. This discretization reduces the continuous singularity distribution to a finite number of unknown potentials or source strengths. The integral equation Eq. (1) and Eq. (2) is then satisfied at collocation points located at the null points of each panel. This gives a system of algebraic equations which are solved for the unknown potentials or source strengths. At each time step the new value of the potentials or source strengths is determined on each quadrilateral panel.

The evaluation of the Rankine source type terms (e.g. $1/r, 1/r'$) in Eq. (1) and Eq. (2) is analytically integrated over quadrilateral panels using the method and formulas of Hess and Smith (1964). For small values of r the integrals are done exactly whilst for intermediate values of r a multi-pole expansion is used. For large values of r a simple monopole expansion is used. The surface and line integrals over each quadrilateral element involving the wave term of the transient free surface Green function $\tilde{G}(P,Q,t,\tau)$ are solved analytically (Liapis 1986, King 1987, Kara 2000) and then integrated numerically using a coordinate mapping onto a standard region and Gaussian quadrature. For surface elements the arbitrary quadrilateral element is first mapped into a unit square. A two-dimensional 2x2 Gaussian quadrature formula is then used to numerically evaluate the surface integrals and 16 points Gaussian quadrature for line integrals. The line integral is evaluated by subdividing $\Gamma(t)$ into a series of straight line segments. The source strength $\sigma(t)$ or potential on a line segment is assumed equal to the source strength or potential of the panel underneath it.

The memory part of the Green function is given as $\tilde{G}(P,Q,t-\tau) = \sqrt{g/r'^3}\,\tilde{G}(\mu,\beta)$ where $\tilde{G}(\mu,\beta) = 2\int_0^\infty d\lambda\sqrt{\lambda}\sin(\beta\sqrt{\lambda})e^{-\lambda\mu}J_0(\lambda\sqrt{1-\mu^2})$ where $\lambda = kr', \mu = -(z+\varsigma)/r'$, and $\beta = \sqrt{g/r'}\,(t-\tau)$. λ is the relative position coordinate between field and source points. The non-dimensional parameter μ is the relative non-dimensional vertical coordinates and varies from zero to one. The non-dimensional parameter β depends on time and represents the phase of the generated waves. The evaluation of the memory part of the transient free surface Green function and its derivatives with an efficient and accurate method is one of the most important elements of the present study. Depending on the values of (μ,β), and t, the following five different methods are used to evaluate memory part $\tilde{G}(\mu,\beta)$; power series expansion, asymptotic expansion, Filon integration quadrature, Bessel function, and asymptotic expansion of complex error function.

3. ITU-WAVE transient wave-structure interaction numerical code

The hydrodynamics functions and parameters in the present paper are predicted with in-house ITU-WAVE transient three-dimensional direct time domain computational code. ITU-WAVE transient wave-structure interaction numerical code which is coded using C++ was validated against experimental, analytical, and other published numerical results (Kara and Kara et.al. 2000 -2017) and used to predict the seakeeping characteristics of mono- and multi-hull floating bodies (e.g. radiation and diffraction), motions, resistance, added-resistance, hydroelasticity of the floating bodies, wave power absorption from ocean waves with latching control, wave energy converter arrays.

4. Comparison of potential (direct) and source (indirect) approaches

The hydrodynamic problem can be solved either potential (direct) or source (indirect) approximation (Kara 2000). If the fluid velocities are required, it is better to use source formulation as this approach gives the fluid velocities directly on the body surface whilst potential formulation requires gradient of potential which is not easy to obtain directly. As the present numerical code ITU-WAVE has the capability to use both potential and source formulations, the comparison between these approaches will be presented to find out the convergence rate of these two approaches against analytical result of hemisphere heave Impulse Response Function (IRF). The analytical heave IRF is obtained by inverse Fourier transform of damping coefficients of Hulme (1982).

Fig. 1(left) shows convergence of heave IRF for hemisphere at Fn = 0.0 with potential formulation. As can be observed from Fig. 1(left) the oscillations at larger times are almost completely eliminated with increasing panel numbers at non-dimensional time step size t*sqrt(g/R) of 0.05. This was the expected result as discussed by many authors (Adachi and Ohmatsu 1979, Newman 1985, Beck and Liapis 1987) when the potential formulation is used for the prediction of IRFs.
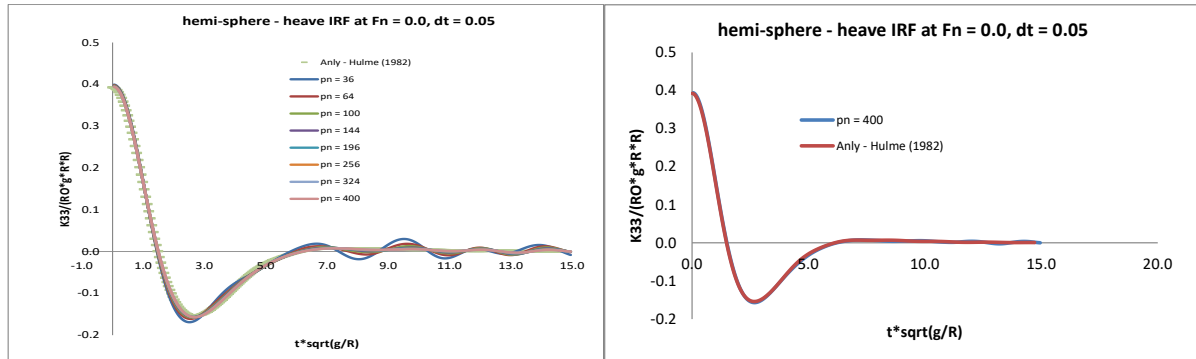

Fig. 1: Convergence of potential formulation heave IRF at a range of panel numbers, Fn = 0.0 and non-dimensional time step size 0.05 for hemisphere

Fig. 1(right) compares present potential formulation results with analytical results of Hulme (1982). It can be seen from Fig. 1(right) the present results with panel number pn = 400 and non-dimensional time step size of 0.05 are almost identical with analytical results of Hulme (1982) and oscillations at larger times are almost eliminated at this panel number.

Fig. 2(left) shows convergence of heave IRF for hemisphere at Fn = 0.0 with source formulation. As can be observed from Fig. 2(left) the oscillations at larger times are not eliminated significantly with increasing panel numbers at non-dimensional time step of 0.05 compared to potential formulation Fig. 1(left) when the same panel numbers are used as in potential approximation.
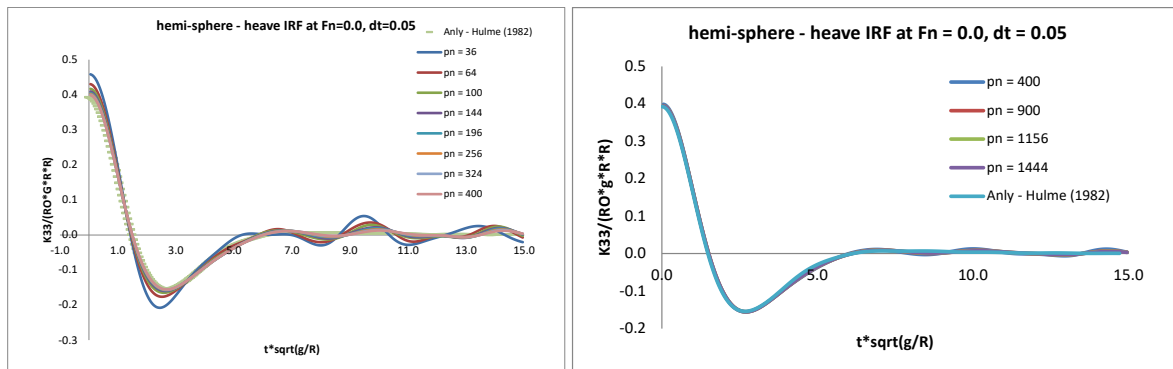

Fig. 2: Convergence of source formulation heave IRF at a range of panel numbers, Fn = 0.0 and non-dimensional time step size of 0.05 for hemisphere

If the panel numbers are significantly increased as seen in Fig. 2(right), the oscillations at larger times are considerably reduced if it is not completely eliminated in source formulation. Fig. 2(right) shows that significant number of panel numbers is required in the case of source formulation compared to potential approximation if one wants to have the same accuracy for both approximations.

Fig. 3(left) shows comparison of potential and source formulations against analytical result of Hulme (1982). Panel number pn = 400 is used for potential formulation whilst it is pn = 1444 for source formulation. It can be seen in Fig. 3(left) the results are almost identical even in larger times although the number of panels for discretization is significantly larger for source formulation compared to potential approximation in order to get the same level of accuracy against analytical result.
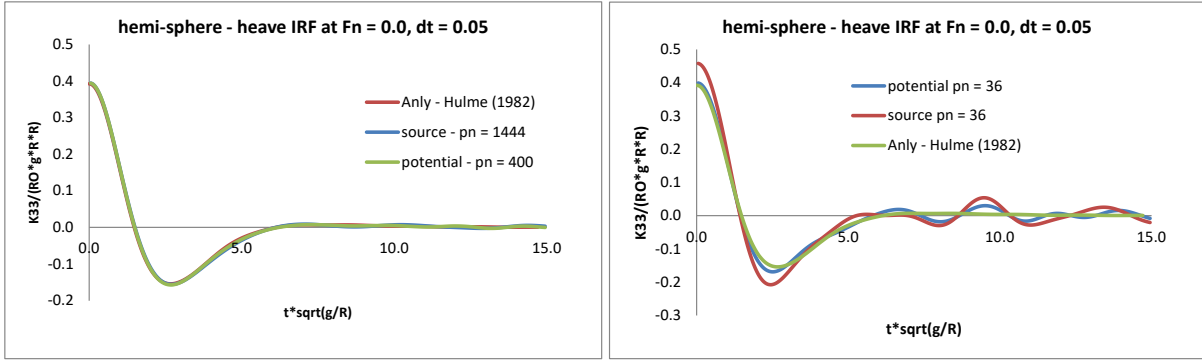
Fig. 3: Comparison of potential and source formulations heave IRFs at Fn = 0.0 and non-dimensional time step size of 0.05 for hemisphere

Fig. 3(right) compare source and potential formulation against analytical results of Hulme (1982) with panel number pn = 36 and non-dimensional time step size of 0.05. As can be seen from Fig. 3(right) even with very small panel number potential formulation result is comparable to analytical result while source formulation result shows large difference at both lower and larger times. This result shows that potential formulation approximates the analytical result much better if small panel numbers are used.

5. Equation of motion

A right-handed coordinate system is used to define the fluid action and a Cartesian coordinate system $\vec{x} = (x, y, z)$ is fixed to the body which is used for the solution of the linearized problem in time domain Fig. 4. Positive x-direction is towards the forward, positive z-direction points upwards, and the z=0 plane (or xy-plane) is coincident with calm water. The bodies undergo oscillatory motion about their mean positions due to incident wave field. The origin of the body-fixed coordinate system $\vec{x} = (x, y, z)$ is located at the centre of the xy plane. The solution domain consists of the fluid bounded by the free surface $S_f(t)$, the body surface $S_b(t)$, and the boundary surface at infinity S_∞ Fig. 4 (Kara 2000).
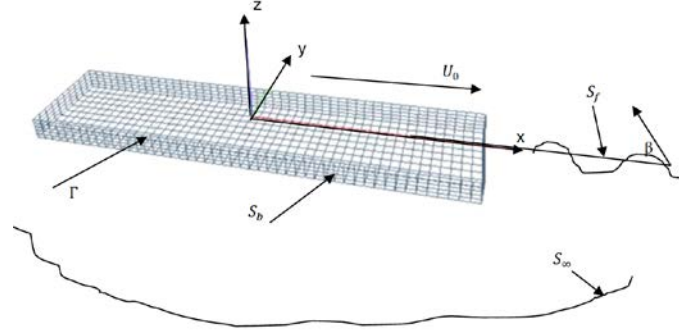

Fig. 4: Coordinate system and surface of the wave energy converters

The following assumptions are taken into account in order to solve the physical problem. If the fluid is unbounded (except for the submerged portion of the body on the free surface), ideal (inviscid and incompressible), and its flow is irrotational (no fluid separation and lifting effect), the principle of mass conservation dictates the total disturbance velocity potential $\Phi(\vec{x}, t)$. This velocity potential is harmonic in the fluid domain and is governed by Laplace equation everywhere in the fluid domain as $\nabla^2 \Phi(\vec{x}, t) = 0$ and the disturbance flow velocity field $\vec{V}(\vec{x}, t)$ may then be described as the gradient of the potential $\Phi(\vec{x}, t)$ (e.g. $\vec{V}(\vec{x}, t) = \nabla \Phi(\vec{x}, t)$).

The dynamics of a floating body's unsteady oscillations are governed by a balance between the inertia of the floating body and the external forces acting upon it. This balance is complicated by the existence of radiated waves which results from due to the oscillations of the bodies and the scattering of the incident waves. This means that waves generated by the floating bodies at any given time will persist indefinitely and the waves of all frequencies will be generated on the free surface. These generated waves, in principle,

6

affect the fluid pressure field and hence the body force of the floating bodies at all subsequent times. This situation introduces memory effects and is described mathematically by a convolution integral. Having assumed that the system is linear, the equation of motion of any floating bodies may be written in a form (Cummins 1962)

$$\sum_{k=1}^{6}(M_{jk}+a_{jk})\ddot{x}_k(t)+b_{jk}\dot{x}_k(t)+(C_{jk}+c_{jk})x_k(t)+\int_0^t d\tau\, K_{jk}(t-\tau)\dot{x}_k(t)=\int_{-\infty}^{\infty}d\tau\, K_{jD}(t-\tau)\zeta(\tau)\quad ;j=1,2,\dots,6$$

(4)

The displacement of the floating bodies from its mean position in each of its rigid-body modes is given $x_k(t)$ in Eq. (4) and the overdots indicate differentiation with respect to time. The time dependent radiation force Eq. (4) is composed of the time independent hydrodynamic coefficients and time dependent impulse response functions. The hydrodynamic coefficients in Eq. (4) a_{jk}, b_{jk}, and c_{jk} account for the instantaneous forces proportional to the acceleration, velocity, and displacement, respectively. The coefficient a_{jk} is the time and frequency independent constant and depends on the body geometry and is related to added mass. The coefficients b_{jk} and c_{jk}, which depend on the body geometry and forward speed, are the time and frequency independent constants and are related to damping and hydrostatic restoring coefficient, respectively.

$$a_{jk}(P)=\rho\iint_{S_0}dS_Q\psi_{1k}(Q)n_j \qquad (5)$$

$$b_{jk}(P)=\rho\iint_{S_0}dS_Q\big(\psi_{1k}(Q)m_j-\psi_{2k}(Q)n_j\big) \qquad (6)$$

$$c_{jk}(P)=-\rho\iint_{S_0}dS_Q\psi_{2k}(Q)m_j \qquad (7)$$

The instantaneous potential $\psi_{1k}(P)$ represents the instantaneous fluid response to the motion of the body. If the body moves and suddenly stops, the entire fluid motion associated with the $\psi_{1k}(P)$ potential stops. The time independent impulsive potential $\psi_{2k}(P)$ represents the potential due to the steady displacements. In other words, if the body is given a unit impulsive velocity in *k-th* mode, the floating body will have a unit displacement in that mode (Ogilvie 1964).

5.1. Radiation Impulse Response Functions (IRFs)

The radiation impulse response (or memory) function $K_{jk}(t)$ is the force on the body in j-th direction due to an impulsive velocity in k-th direction. The memory function $K_{jk}(t)$ accounts for the free surface effects which persist after the motion occurs and $K_{jk}(t)$ is the time dependent part and depends on body geometry, forward speed, and time. It contains the memory effect of the fluid response. The convolution integral in Eq. (4), whose kernel is a product of the radiation impulse response function $K_{jk}(t)$ and velocity of the floating body $\dot{x}_k(t)$, is a consequence of the radiated wave of the floating body. When this wave is generated, it affects the floating body at each successive time step (Ogilvie 1964).

$$K_{jk}(P,t)=\rho\iint_{S_0}dS_Q\left\{\frac{\partial}{\partial t}\chi_k(Q,t)n_j-\chi_k(Q,t)m_j\right\} \qquad (8)$$

The time dependent memory potential $\chi_k(t)$ represents the transient potential, which results from the effect of the free surface. In the case of the transient problem, all motions die out after a reasonable time and all displacements approach zero asymptotically. In other words, the transient potential $\chi_k(t)$ is the velocity potential of the motion which results from the impulse of the floating body velocity at time $t=0$. The time independent impulsive potentials $\psi_{1k}(P)$ and $\psi_{2k}(P)$ provide initial conditions on the potentials which describe the transient motion $\chi_k(t)$ (Ogilvie 1964).

A modified Wigley I hull form with forward speed which has parabolic sections is used for numerical analysis. This Wigley I hull form has the length to beam ratio $L/B = 10$, length to draft ratio $L/T = 16$. Wigley I hull form (which has 3.0m length and is used in the experimental study of Journee (1992)) is used for the validation of ITU-WAVE numerical results. It is assumed Wigley I hull form, which is free for heave and pitch modes and fixed for other modes, is studied to predict motions at Fn = 0.30 and head seas $\beta = 180^0$. The underwater part of Wigley I hull form is defined analytically and is given by the equation.

$$\eta = (1 - \varsigma^2)(1 - \xi^2)(1 + 0.2\xi^2) + \varsigma^2(1 - \varsigma^8)(1 - \xi^2)^4 \quad (9)$$

where $\eta = 2y/B$, $\xi = 2x/L$, and $\varsigma = z/T$ and L, B, T are length, beam, and draft of the floating body, respectively. The last term in the equation Eq. (9) is the modification compared to the original Wigley I hull form.
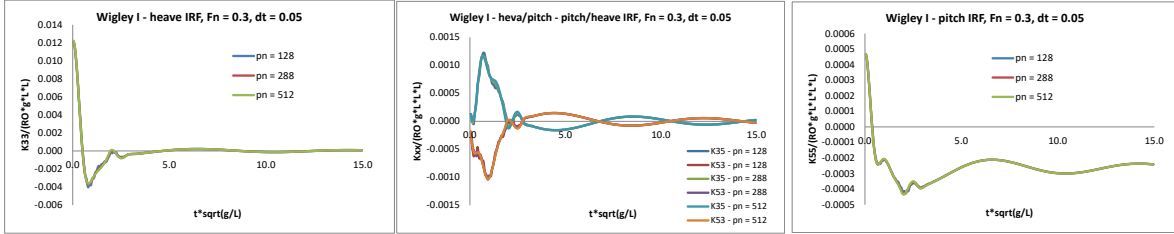

Fig. 5: Wigley I hull form with L/B=10 and L/T=16, non-dimensional radiation heave, heave-pitch / pitch heave cross-coupling and pitch IRFs at Fn = 0.3 – potential approach

Fig. 5 shows the convergence test of radiation IRFs for heave and pitch modes. As Wigley I hull form is symmetric in terms of xz-coordinate plane of the reference coordinate system, only half of hull form is discretized for numerical analysis. Numerical experience showed that numerical results are not very sensitive in terms of non-dimensional time step size $t * sqrt(g/L)$ of 0.01, 0.03, and 0.05 over the range of panel numbers of 128, 288, 512 whilst the numerical results are sensitive in terms of panel numbers as can be seen in Fig. 5. The results at panel number 288 is converged and used for the present ITU-WAVE numerical calculations with the non-dimensional time step size of 0.05. Potential approach is used for better prediction as only potential and its time derivatives are required for IRFs predictions.

5.2. Diffraction Impulse Response Functions (IRFs)

The transient generalized exciting force including Froude-Krylov and diffraction forces in the presence of an incident wave field acting on the body surface in the j-th direction may be written in a form which is essentially proposed by King (1987).

$$F_{jD}(t) = \int_{-\infty}^{\infty} d\tau K_{jD}(t - \tau)\zeta(\tau) = \int_{-\infty}^{\infty} d\tau\{K_{jS}(t - \tau) + K_{jI}(t - \tau)\}\zeta(\tau) \quad (10)$$

$$K_{jI}(t) = \iint_{S_0} dS_Q \hat{p}(t)n_j \quad (11)$$

$$K_{jS}(t) = \rho \iint_{S_0} dS_Q \left\{ -\frac{\partial}{\partial t}\widehat{\phi}_S(t)n_j + \widehat{\phi}_S(t)m_j \right\} \quad (12)$$

The term $K_{jD}(t)$ in Eq. (10) has two components representing the exciting forces and moments due to the diffraction and Froude-Krylov forces, respectively. The forces are due to the incident wave elevation $\zeta(t)$ and the kernel $K_{jD}(t)$ is the diffraction IRFs which are the forces on the body in the j-*th* direction due to a uni-directional impulsive wave elevation with a heading angle β (Fig. 4). The kernels $K_{jS}(t)$ and $K_{jI}(t)$ are the IRFs for diffraction (scattering) and Froude-Krylov forces, respectively and are of the form which corresponds to a time-invariant linear system since the reference point of the waves is fixed with respect to the moving floating body. $\hat{p}(t)$ is the IRF for the pressure calculation and $K_{jI}(t)$ is found by direct

8

integration of the $\hat{p}(t)$ over the floating body surface. The scattering (diffraction) perturbation potential $\hat{\phi}_S(t)$, which is obtained by the solution of Eq. (1) or Eq. (2), represents the diffracted wave potential due to an impulsive incident wave (King 1987). Fig. 6 shows the convergence test of the exciting IRFs for heave and pitch modes. As in radiation problem, IRFs in Fig. 6 are converged at panel number pn = 288 and non-dimensional time step size of 0.05.
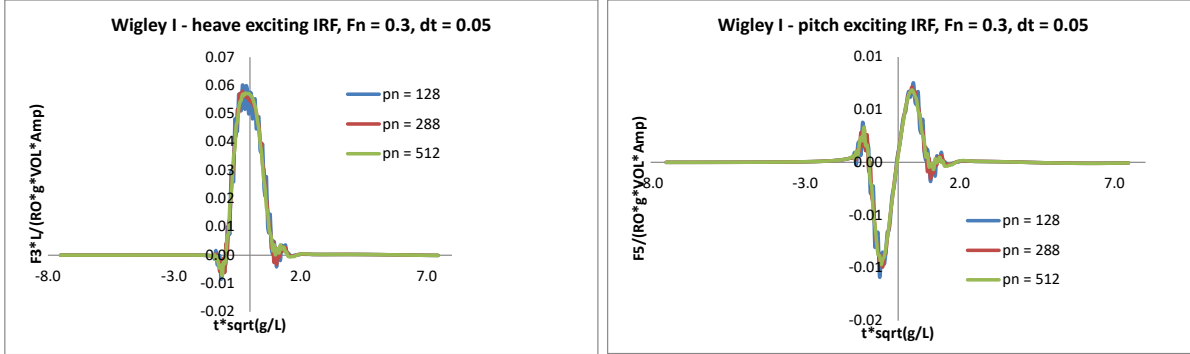

Fig. 6: Wigley I hull form with L/B=10, L/T=16, non-dimensional exciting heave and pitch IRFs at Fn = 0.30 and $\beta = 180^0$ – potential approach

The excitation of the floating body is provided by the incident wave $\zeta(t)$, which is the arbitrary wave elevation at the body-fixed coordinate system and measured at the origin of the coordinate system Fig. 4. The incident wave potential which is known and given as (King 1987)

$$\varphi_I(\vec{x}, t) = \frac{ig}{\omega} e^{k(z - i\varpi)} e^{i\omega_e t} \quad (13)$$

where the encounter frequency is given as $\omega_e = \omega - U_0 k \cos(\beta)$, ω the absolute frequency of the linear system, β the angle of the wave propagation direction with the positive x −direction, k the wave number and is related to the absolute frequency ω (in the case of infinite depth) by $k = \omega^2/g$, and $\varpi = x\cos(\beta) + y\sin(\beta)$ which is the total distance in the wave direction. It is assumed that the incident wave potential Eq. (13) is a uni-directional wave system which contains all frequencies, and it describes a wave elevation which is Dirac delta function $\delta(t)$ in time when it is viewed from the origin of the body-fixed coordinate system Fig. 4.

5.3. Response Amplitude Operators (RAOs)

Once the inertia matrix, restoring matrix and fluid forces e.g. radiation and diffraction forces are known, the equation of motion of floating body Eq. (4) may be solved using the fourth order Runge-Kutta method. The experimental results of Journee (1992) for heave and pitch RAOs at Fn = 0.30 and $\beta = 180^0$ are compared with ITU-WAVE numerical results in Fig.7.
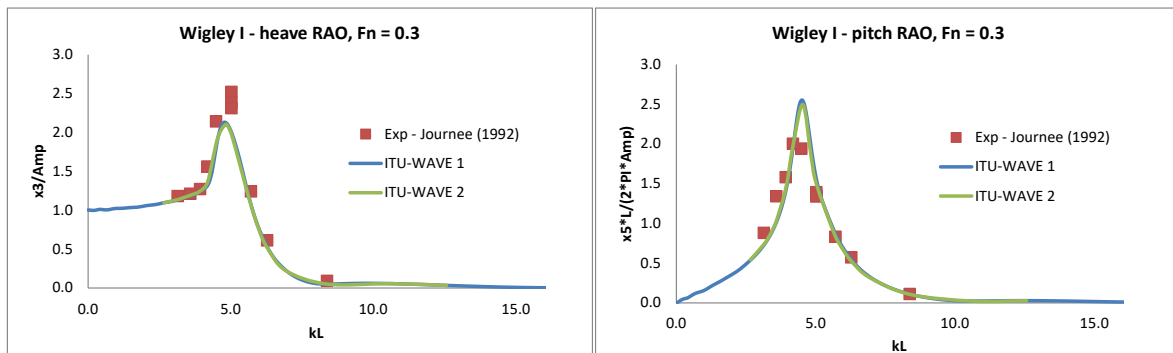

Fig. 7: Wigley I hull form with L/B=10, L/T=16, non-dimensional heave and pitch RAOs at Fn = 0.30 and $\beta = 180^0$ – potential approach

Two different approaches are used in order to get ITU-WAVE numerical results. Firstly RAOs are obtained by the time marching of the Eq. (4) for each encounter frequency and these results are represented as ITU-WAVE 2 in Fig.7. Secondly, the frequency domain version of equation of motion is used for which the frequency dependent added mass, damping coefficients and exciting forces are obtained by the use of Fourier transform of radiation IRFs Fig. (5) and exciting IRFs Fig. (6), respectively. ITU-WAVE heave and pitch RAOs results from the solution of frequency domain equation of motion are presented as ITU-WAVE 1. As can be seen from Fig. 7, the numerical results from time domain and frequency domain solutions of ITU-WAVE have perfect match as expected.

5.4. Asymptotic Continuation

The decay of the forward speed IRFs in time is different from that of zero speed IRFs due to the resonance at the critical reduced frequency $\tau = \omega_c U/g = 1/4$. The impulse acting on the floating body generates energy due to the presence of the wave system. This energy at the group velocity of wave components propagates away from the floating body at zero-forward speed whilst in the case of forward speed, this energy remains in the vicinity of the floating body since the group velocity of the wave component is approximately equal to the speed of the floating body. For the long simulation of the floating bodies, it is very important to avoid the computation of transient free-surface wave Green function, which is computationally expensive and results in the prediction of IRFs for each mode and at each time step. In ITU-WAVE numerical code, the computation of forward speed IRFs are truncated at the non-dimensional time step of $15\sqrt{g/L}$ and the asymptotic values of each IRFs are approximated (Bingham et.al. 1994) as $t \rightarrow \infty$

$$K_{jk}(t) \approx a_0 + \frac{1}{t}[a_1 \cos(\omega_c t) + a_2 \sin(\omega_c t)] \quad (14)$$

The constants in Eq. (14) can be determined by a Least Squares fit. Fig. (8) shows comparison between a very long calculation of the heave IRFs and asymptotic continuation results.
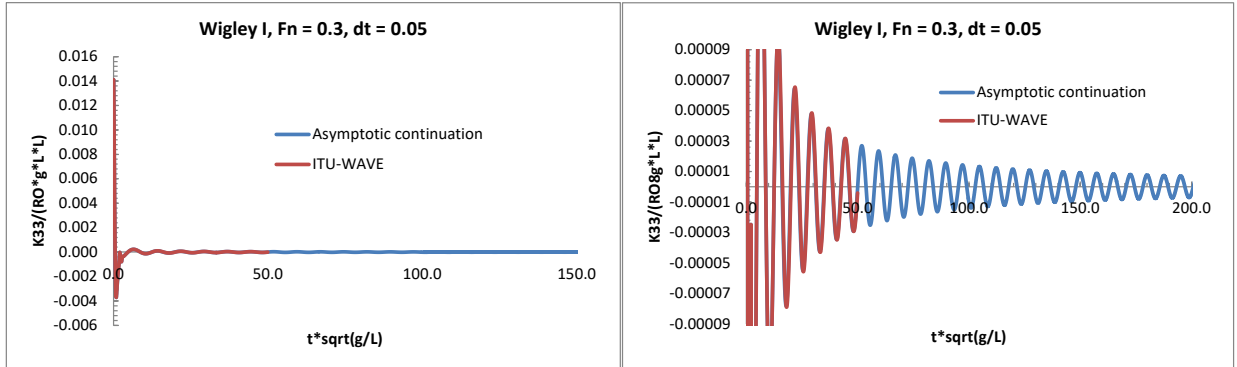

Fig. 8: Comparison (left) and expanded view (right) of heave IRF of Wigley I hull form at F_n=0.30 between the solution of integral equation Eq. (1) and asymptotic continuation – potential formulation

The solution of the time domain discretized integral equations demonstrates an oscillation over longer time as shown in expanded view of the heave IRF in Fig. (8). The oscillatory error at large time is apparently the result of the integral equation Eq. (1) method of solution and not numerical inaccuracies. The oscillatory error in the time domain discretized integral equations is the equivalence of the irregular frequencies in the frequency domain. The oscillation amplitude decreases when forward speed increases. The oscillation amplitude at both zero and forward speed cases can be reduced by increasing panel numbers and by decreasing the time step size (Fig. (1) and Fig. (2)).

6. The First Order Steady Forces

The steady perturbation potential $\varphi(P, t)$ may be solved as the steady state limit of the transient radiation problem. In the case of the steady state limit, time t goes to infinity $t \rightarrow \infty$. The steady state wave forces on the body surface due to its steady translation may be written as

$$F_{Sj}(t) = \rho U \iint_{\bar{S}_b} dS_Q \frac{\partial}{\partial x} \varphi_1(Q,t) n_j \quad (15)$$

where $\varphi_1(P,t)$ is the surge radiation perturbation potential at x-direction, U forward speed of floating body. ITU-WAVE numerical results are presented for the analytically defined Wigley R hull form with length to beam ratio $L/B = 10$ and length to draft ratio $L/T = 16$. The half beam of the Wigley R hull form is given as

$$\eta = (1 - \varsigma^2)(1 - \xi^2) \quad (16)$$

where $\eta = 2y/B$, $\xi = 2x/L$, and $\varsigma = z/T$ and L, B, T are length, beam, and draft of the floating body, respectively. As mentioned before the steady perturbation potential can be considered steady state limit of transient impulsive velocity of surge radiation problem with forward speed. As the quantity of the steady problem (e.g. steady wave resistance, sinkage force and trim moment) are an order of magnitude smaller than the transient response, convergence test of the steady problem are presented in Fig. (9). As the prediction of the first order steady forces Eq. (15) requires the fluid velocity in x-direction, the source formulation Eq. (3), which gives fluid velocities directly, is used to obtain the steady forces.
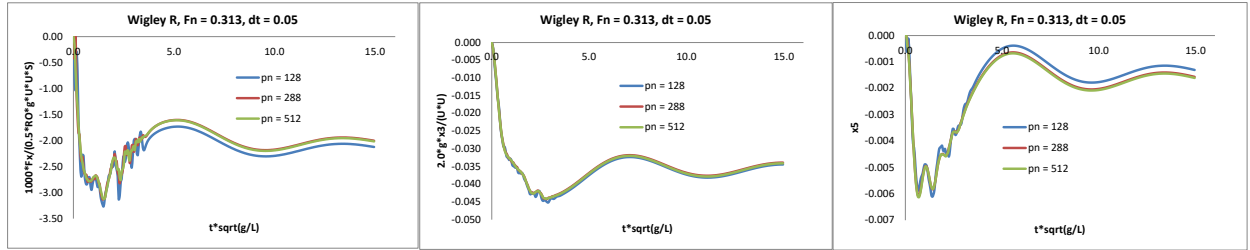

Fig. 9: Convergence of the steady wave resistance, sinkage force and trim moment of Wigley R hull form at a range of different panel numbers at Fn=0.313 and time step size 0.05 – source formulation

As in convergence of the first order wave forces in section 5 (e.g. radiation and diffraction IRFs), ITU-WAVE numerical results are not very sensitive in terms of non-dimensional time step size $t * sqrt(g/L)$ of 0.01, 0.03, and 0.05 over the range of panel numbers of 128, 288, 512 whilst the numerical results are sensitive in terms of panel numbers as can be seen in Fig. 9 and the results at panel number 288 is converged and used for the present ITU-WAVE numerical calculations with the non-dimensional time step size of 0.05.

The floating body starts its motion at rest and reaches a constant speed U with direction of the speed parallel to the free surface in the first order steady force calculation. After some oscillation the force takes a constant value, which is the resistance of the body, but it is computationally expensive to reach the steady state limit value of the transient impulsive velocity potential. After obtaining the regular oscillation, the remaining portion of the calculation may be fitted using asymptotic continuation Eq. (14) in order to avoid computationally expensive transient free-surface Green function calculation. It is assumed that the first order steady force values are decaying with 1/t in time in Eq. (14). This approximation agrees with Wehausen (1964) who investigated the effects of the initial transients on the wave resistance of a thin ship starting abruptly from rest.
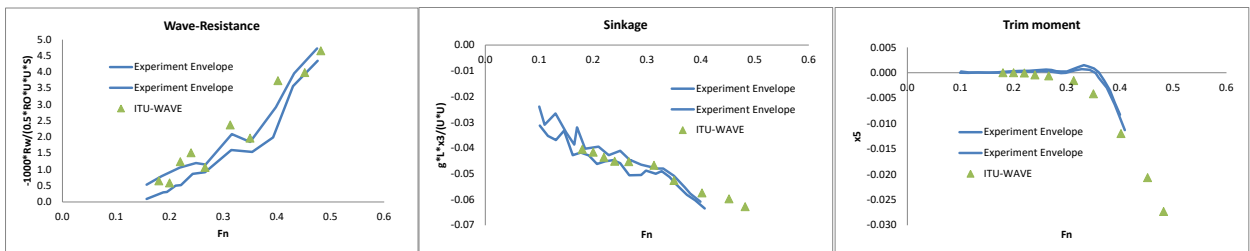

Fig. 10: Variation of wave resistance, sinkage force and trim moment of Wigley R form at a range of different Froude number – source approach

11

Fig. 10 shows the steady wave resistance, sinkage force and trim moment of Wigley R hull form over a range of Froude numbers. ITU-WAVE numerical results are calculated for the fixed model condition whilst the experimental envolope results are given for free trim and sinkage condition as well as free sinkage and fixed trim moment. The wave resistance experimental envelope results are obtained from McCarthy (1979) whilst the experimental envelope for sinkage force and trim moment is from Noblesse (1983). ITU-WAVE numerical calculations were undertaken up to non-dimensional time step of $15\sqrt{g/L}$ and then asymptotic continuation Eq. (14) was used to obtain the asymptotic value of steady wave resistance, sinkage force and trim moment.

7. Multi-body Interactions

Two truncated vertical cylinder is used for numerical analysis as a first test case for multi-body interactions. It is assumed two cylinders have the same draft and radius R although present method can be applied for different draft and radius. The truncated cylinders have the radius of R, draft of 2R and hull separation to diameter ratio of d/D=1.3. It is assumed that two truncated cylinders are free for sway mode and fixed for other modes. These two truncated cylinders are studied to predict sway radiation and diffraction IRFs in time and added-mass, damping coefficients, and exciting force in frequency domain. ITU-WAVE numerical results for sway added-mass, damping coefficients and exciting force (which are the sum of the diffraction and Froude-Krylov forces) with Fn = 0.0 and heading angle $\beta = 90^0$ are compared with the analytical results (Kagemoto and Yue 1986).

Fig. 11 shows the convergence test of radiation and diffraction IRFs for sway mode. As two truncated vertical cylinders are symmetric in terms of xz-coordinate plane of the reference coordinate system, only single hull form is discretized for numerical analysis. Numerical experience showed that numerical results are not very sensitive in terms of non-dimensional time step size $t * sqrt(g/L)$ of 0.01, 0.03, and 0.05 over the range of panel numbers of 128, 200, 288 on single body of two truncated vertical cylinder whilst the numerical results are quite sensitive in terms of panel numbers as can be seen in Fig. 11 and the results at panel number 200 on single hull form is converged and used for the present ITU-WAVE numerical calculations for both two and single truncated vertical cylinder with the non-dimensional time step size of 0.05.
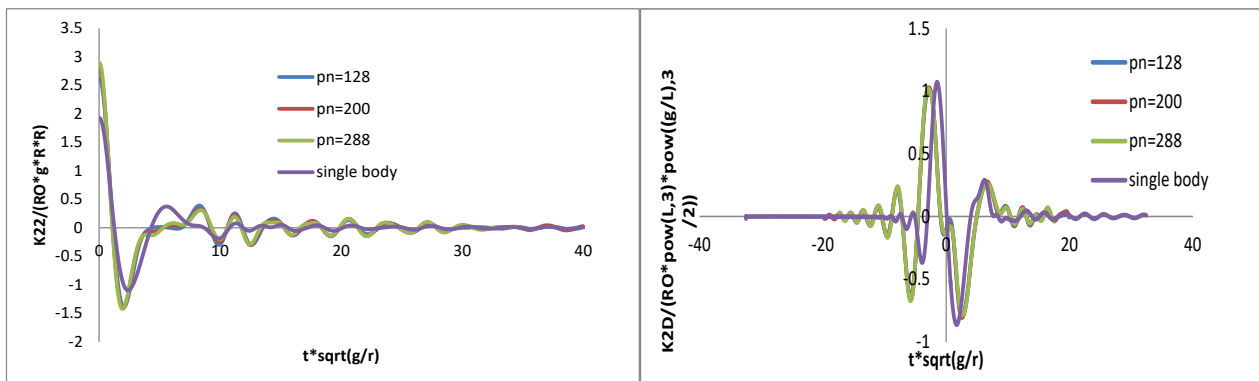

Fig. 11: Two truncated vertical cylinder - non-dimensional radiation $K_{22}(t)$ and diffraction sway $K_{2D}(t)$ IRFs at Fn = 0.0, d/D = 1.3 and beam seas $\beta = 90^0$ – Potential approach

It may be noticed that the magnitude of radiation IRFs of two cylinder in sway mode Fig. 11 is quite big compared to single cylinder. The other distinctive difference of IRF of single and two cylinders in Fig. 11 is the behaviour of radiation IRFs function in longer times in sway mode. IRF of two cylinders have oscillations over longer times with decreasing amplitude while single cylinder IRF decays to zero just after first oscillation. This behaviour of IRF implicitly means that the energy between two cylinders is trapped in the gap and only a minor part of the energy is radiated outwards each time when the wave is reflected off the hull while all energy is dissipated in the case of single cylinder. It is expected that geometry of two bodies would significantly affects the radiated, diffracted, and trapped waves which result from due to standing

waves in the gap. In the case of diffraction IRF in Fig. 11, there are no significant differences in sway mode between single and two cylinders' IRFs except slight shift.

As mentioned previously the time domain radiation force coefficients are related to the frequency domain force coefficients through Fourier transform when the motion is considered as a time harmonic motion. The Fourier transform of radiation and exciting IRFs in time domain gives the frequency dependent added mass and damping coefficients as well as exciting force in frequency domain, respectively and may be written as

$$A_{jk}(\omega) = a_{jk} - \frac{1}{\omega}\int_0^t d\tau K_{jk}(\tau)\sin(\omega\tau) - \frac{c_{jk}}{\omega^2} \qquad (17)$$

$$B_{jk}(\omega) = b_{jk} + \int_0^t d\tau K_{jk}(\tau)\cos(\omega\tau)$$

$$F_j(\omega) = \int_{-\infty}^{+\infty} d\tau \left[K_{jl}(\tau) + K_{jS}(\tau)\right] e^{-i\omega`\tau`} \qquad (18)$$

where the coefficients $A_{jk}(\omega)$ and $B_{jk}(\omega)$ are the frequency dependent added mass and damping coefficients, respectively whilst $F_j(\omega)$ is the complex exciting force. Added-mass $A_{22}(\omega)$, damping coefficients $B_{22}(\omega)$ and exciting force amplitude $F_2(\omega)$ in Fig. 12 is obtained by Fourier transform of radiation sway IRF K₂₂(t) and diffraction sway IRF K₂D(t) of Fig. 11, respectively.
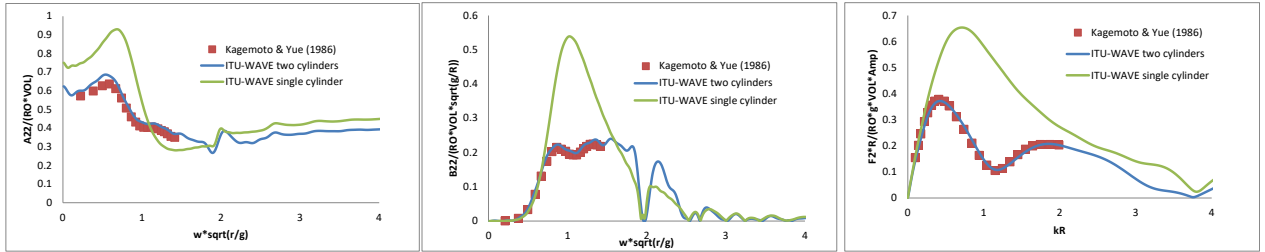

Fig. 12: Two truncated vertical cylinders - non-dimensional sway added-mass, damping coefficients and exciting force amplitude (beam seas $\beta = 90^0$) at Fn = 0.0 and d/D = 1.30 – potential approach

ITU-WAVE numerical results of added-mass and damping coefficients in sway mode of two cylinders are satisfactory agreement with the analytical prediction (Kagemoto and Yue 1986) as can be seen in Fig. 12. In addition to two cylinders added-mas and damping coefficients in Fig. 12, the single cylinder results are presented as the comparison with two cylinders results. It can be seen in Fig. 12 the behaviours of two cylinders results are significantly different from those of single cylinder due to trapped waves and hydrodynamic interactions in the gap of two cylinders.

The effects of diffraction hydrodynamic interactions in sway mode (at which interactions are effective in the whole frequency range) are stronger in Fig. 12. These interaction effects in sway mode are even stronger in a limited frequency range which is of interest for the motions of the bodies in array systems and is around kR =0.5 and kR = 2.0 of non-dimensional frequency in radiation and diffraction sway mode in Fig. 12, respectively.

7.1. Four truncated vertical cylinder arrays

Four truncated vertical cylinder is used for numerical analysis as the second test case for multi-body interactions. As in two cylinders, it is assumed four cylinders have the same draft and radius. Four truncated cylinders have the radius of R and draft of 2R and hull separation to diameter ratio d/D=2.0. It is assumed that four truncated cylinders are free for sway mode and fixed for other modes and are studied to predict sway added-mass, damping coefficients and exciting force amplitude in frequency domain. ITU-WAVE numerical results for sway added-mass $A_{22}(\omega)$, damping coefficients $B_{22}(\omega)$ and exciting force amplitude $F_2(\omega)$ with heading angle $\beta = 90^0$ are compared with the analytical results (Kagemoto and Yue 1986) in Fig. 13.
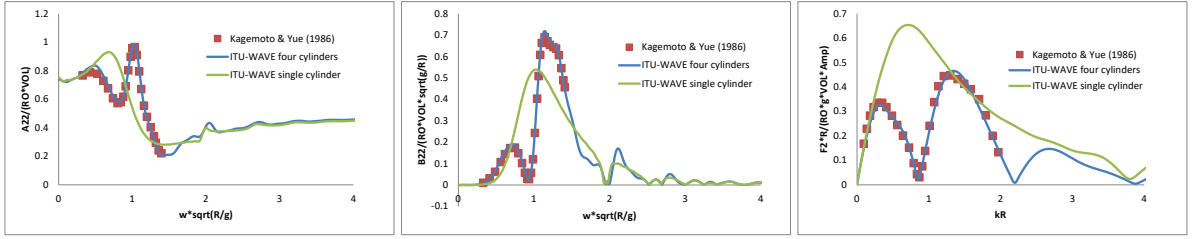
Fig. 13: Four truncated vertical cylinders - non-dimensional sway added-mass, damping, and exciting force amplitude at Fn = 0.0, d/D = 2.0 and beam seas $\beta = 90^0$ – potential approach

There would not be energy transfer or radiated waves from floating body to sea when the damping coefficients are zero as can be observed in Fig. 13. It may be noticed there are three resonances behaviours in damping coefficients in sway mode which implies that high standing waves occur between the maximum and minimum damping coefficients (Ohkusu 1969, van Oortmerssen 1979). It may be noticed the peaks are finite at non-dimensional resonance frequencies as some of the wave energy dissipate under the floating body and radiates to the far field.

8. The second order steady forces

For the prediction of the mean second order forces, the pressure integration method with the Neumann-Kelvin linearization is used in ITU-WAVE numerical code. It is not necessary to solve the second-order boundary value problem even though the forces are second-order quantities in order to calculate the mean second order forces on a floating body in waves. The solution of the second order problem results in mean forces, and forces oscillating with difference frequency and sum frequencies in addition to the linear solution. The fluid pressure is integrated over the hull to obtain the global hydrodynamic forces at each time step. These wave loads will determine the subsequent motion of the body with Eq. (19). Therefore, an accurate and complete description of the pressure is essential in order to properly simulate the response of a body. The second-order force in time domain neglecting the second-order hydrostatic force (since its contribution to mean second order force (or added resistance) prediction is zero) can be written as (Kara 2011)

$$
\begin{aligned}
F_i^{(2)}(t) = &\frac{\rho g}{2} \int_\tau dl \left[\zeta - (\xi_3 + y\alpha_1 - x\alpha_2)\right]^2 \frac{n_i}{\sqrt{1 - n_3^2}} \\
&- \frac{\rho}{2} \iint_{\bar{S}_b} dS_Q \nabla\varphi^{(1)} \cdot \nabla\varphi^{(1)} n_i \\
&- \rho \iint_{\bar{S}_b} dS_Q \left(\vec{\xi} + \vec{\alpha} \times \vec{x}\right) \cdot \nabla\left(\varphi_t^{(1)} - U\varphi_x^{(1)}\right) n_i \\
&\vec{\alpha} \times \left(-\rho \iint_{\bar{S}_b} dS_Q \left(\varphi_t^{(1)} - U\varphi_x^{(1)}\right) n_i\right) \qquad ; \quad i = 1,2,3 \qquad (19)
\end{aligned}
$$

where $\vec{\xi} = (\xi_1, \xi_2, \xi_3) = (x_1, x_2, x_3)$, $\vec{\alpha} = (\alpha_1, \alpha_2, \alpha_3) = (x_4, x_5, x_6)$, upper-scripts $\varphi^{(1)}$ in potential and fluid velocities $\nabla\varphi^{(1)}$ represent the first order quantities whilst $F_i^{(2)}(t)$ is for second order quantity. In Eq. (19), the first line is the contribution from the vertical wave elevation and vertical motion of the floating body that change the wetted surface in the water line region. The second line comes from the quadratic term due to fluid velocities. The third line is the correction from the instantaneous pressure to mean position. The fourth line comes from the correction to body-fixed normal vector $\vec{n}$.
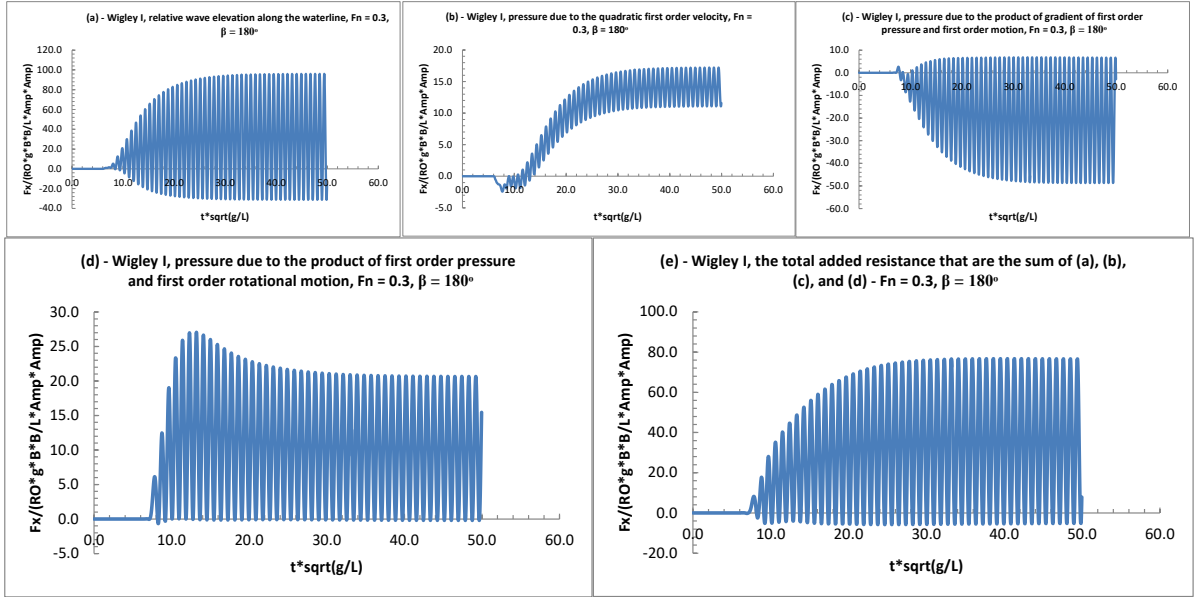
14

Fig 14: achieving steady-state of the added resistance components at the resonance frequency for a Wigley I hull form at F_n =0.3 and β = 180 degrees (a) relative wave elevation along the waterline – the first line of Eq. (19) (b) pressure due to the quadratic first order velocity – the second line of Eq. (19) (c) pressure due to the product of gradient of first order pressure and first order motion – the third line of Eq. (19) (d) pressure due to the product of first order pressure and first order rotational motion – the fourth line of Eq. (19) (e) the total added resistance that are the sum of (a), (b), (c), and (d) – source formulation

Fig. 14 shows the achieving steady-state of each components of the added resistance which is given in Eq. (19) at the resonance frequency and sum of these components for Wigley I hull form at F_n =0.3 and β = 180 degrees. Wigley I hull form in the present mean second-order calculation is free to heave and pitch motions and restrained for the other modes. The mean second order forces $\overline{F_i^{(2)}}$ over a time range T is given as

$$\overline{F_i^{(2)}} = \frac{1}{T}\int_0^T dt\, F_i^{(2)}(t) \quad (20)$$

The averaging time T must be much larger than the characteristics period of the incident wave. Fig. 15 shows the mean added resistance of Wigley I hull form at F_n =0.3 and β = 180 degrees for a range of frequencies. As the second order force prediction Eq. (19) requires the fluid velocities calculations, the source formulation is used with panel number pn=288 and non-dimensional time step of 0.05 as the numerical results are converged at this panel number and time step.
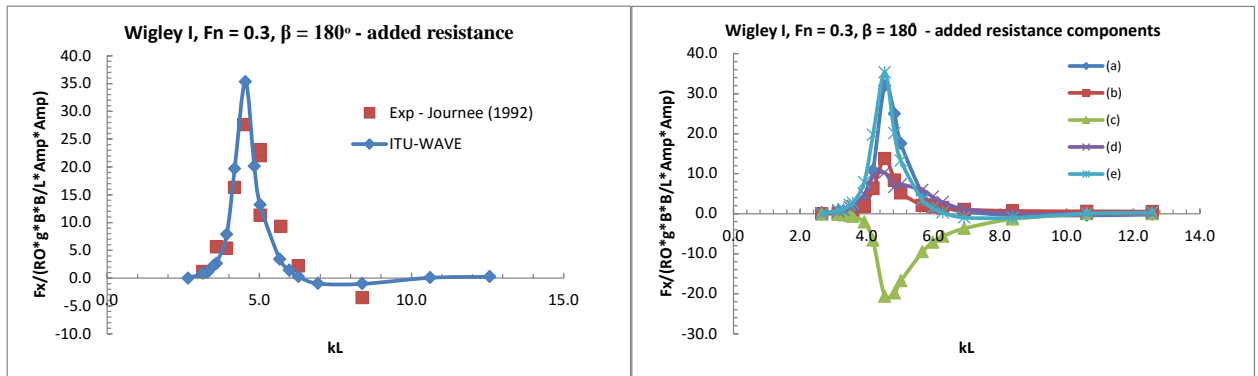

Fig. 15: Non-dimensional mean added resistance (left) and mean added resistance components (right) for a range of non-dimensional frequencies for Wigley I hull form at F_n =0.3 and β = 180', (a) relative wave elevation along the waterline – the first line of Eq. (19) (b) pressure due to the quadratic first order velocity – the second line of Eq. (19) (c) pressure due to the product of gradient of first order pressure and first order motion – the third line of Eq. (19) (d) pressure due to the product of first order pressure and first order rotational motion – the fourth line of Eq. (19) (e) the total added resistance that are the sum of (a), (b), (c), and (d) – source formulation

The experimental results, which are compared with ITU-WAVE numerical results, are taken from Journee (1992). In order to avoid the transient effects, only the last half of the time domain results Fig. 14 are taken into account for the prediction of the mean added resistance using Eq. (20).

9. Hydroelasticity of floating bodies

For hydroelastic analysis, It is assumed that the mass per unit length and structural stiffness EI are uniform along the length and the non-dimensional stiffness parameter is defined as $S = EI/\rho gL^5$ (Newman 2005, Lee and Newman 2000). The link between elastic and stiff structure can be determined using this stiffness parameter S. The stiffness parameter S represents the ratio between structural stiffness and hydrostatic restoring force, where $S = \infty$ corresponds to completely rigid structure whilst $S = 0$ corresponds to completely flexible structure.

9.1. Elastic structures

The flexible barge Fig. 4 has length to beam ratio $L/B = 4.075$, length to draft ratio $L/T = 20.375$, and actual length of the barge is $2.445m$. This flexible barge is studied to predict vertical deflection (RAOs) for the validation of ITU-WAVE numerical results against experimental results (Malenica et.al. 2003) at Fn=0.0 and head seas $\beta = 180^0$. The vertical bending stiffness EI is given as $175\ Nm^2$ in the experimental study which results in non-dimensional stiffness parameter $= EI/\rho gL^5 = 1.99 \times 10^{-4}$. The barge in Fig. 4 is discretized with 1080 panels with 49 panels in longitudinal direction, 10 panels in transverse direction, and 5 panels in vertical direction as the numerical results are converged at this panel numbers and non-dimensional time step size of 0.05.
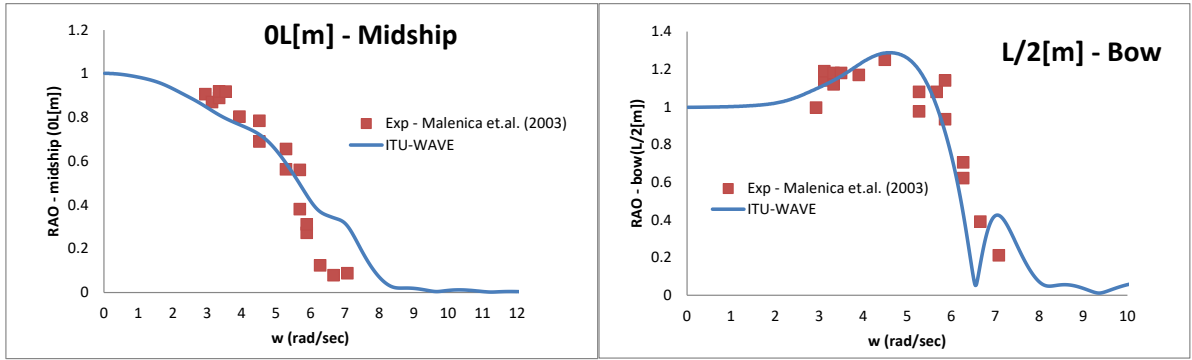

Fig. 16: Barge vertical deflection (RAOs) at mid-ship and bow with stiffness factor $= EI/\rho gL^5 = 1.99 \times 10^{-4}$, Fn = 0.0 and head seas $\beta = 180^0$ – potential approach

Fig. 16 shows the vertical deflection with stiffness factors $S = EI/\rho gL^5 = 1.99 \times 10^{-4}$ at mid-ship and bow. As expected, motion approaches to the unity at low frequencies whilst motion approaches to zero in the case of high frequencies. It can be seen from Fig. 16 the comparisons between present direct time domain ITU-WAVE numerical results and experimental results (Malenica et.al. 2003) are quite satisfactory.

9.2. Stiff structures

Wigley I hull form has length to beam ratio $L/B = 7$, length to draft ratio $L/T = 18$, and actual length $2.5m$. Wigley I hull form (which is free for heave and pitch modes and fixed for other modes) is studied to predict bending moment and shear force experimentally (Adegeest 1994). ITU-WAVE numerical results of shear force and bending moment at Fn=0.2 and head seas $\beta = 180^0$ are compared with experimental results (Adegeest 1994) as Wigley I hull form is considered as a stiff structure. If the contribution of rigid body motion to the pressure field is much higher than elastic modes, the floating body can be considered as stiff which means the floating body does not deform very much compared to the rigid body motions. In other words, in the case of stiff structure it is expected that the amplitude of deformable modes are not significant and the radiation due to these deformable modes can be neglected. The load distribution, which is the derivative of the shear force V, can be written as (Kara 2015)

$$L(q) = \frac{dV}{dq} = \sum_{j=1}^{K} F_j \cdot u_j''''(q) \qquad (21)$$

where F_j Eq. (22) is the unknown force coefficients, K total degree of freedom of elastic structure which include 6 rigid degree-of-freedom, $u_j(q)$ total displacements of the elastic structure. The shear force and bending moment may be found as the first and the second integrations of Eq. (21), respectively.

$$F_j(\omega) = k_{jk}\xi_k(\omega) = X_j(\omega) - \sum_{k=1}^{2} \left\{ -\omega^2 \left(M_{jk} + A_{jk}(\omega) \right) + i\omega B_{jk}(\omega) + C_{jk} \right\} \xi_k(\omega) \qquad (22)$$

where $X_j(\omega)$ is frequency dependent exciting force amplitudes, k_{jk} structural stiffness. In the case of stiff structure, only rigid body effect is taken into account as ξ_k (which is motion amplitudes in frequency domain) for $k > 6$ is assumed to be small when they are compared to rigid body motion. The summation in Eq. (22) implies that rigid body motion parameters and their coupling with elastic modes for added-mass, damping, and restoring coefficients are required for the prediction. Heave and pitch rigid-body modes are represented as 1 and 2, respectively in Eq. (22) as other rigid body modes are restrained. This means that information related to added-mass, damping, and restoring terms in elastic modes due to rigid body motions only (which are coupled with elastic modes) needs to be known for the numerical calculation. The bending moments and shear forces can be predicted by the use of this approach in which the floating body is considered as a long, slender, and stiff beam.

The prediction of global loads including bending moment and shear force requires the mass distribution of floating body. It is assumed that mass is distributed as the local beam as $M_{jk} = \frac{M}{4}\delta_{jk}$ (where M is the total mass of the beam and δ_{jk} is the Kroenecker delta function) and scaled in a way that the weight of the total mass equals the mass of the displaced fluid in ITU-WAVE numerical code. ITU-WAVE numerical results due to this approach for shear force and bending moment at Fn=0.2 and $\beta = 180^0$ are shown in Fig. 17 together with experimental results (Adegeest 1994).
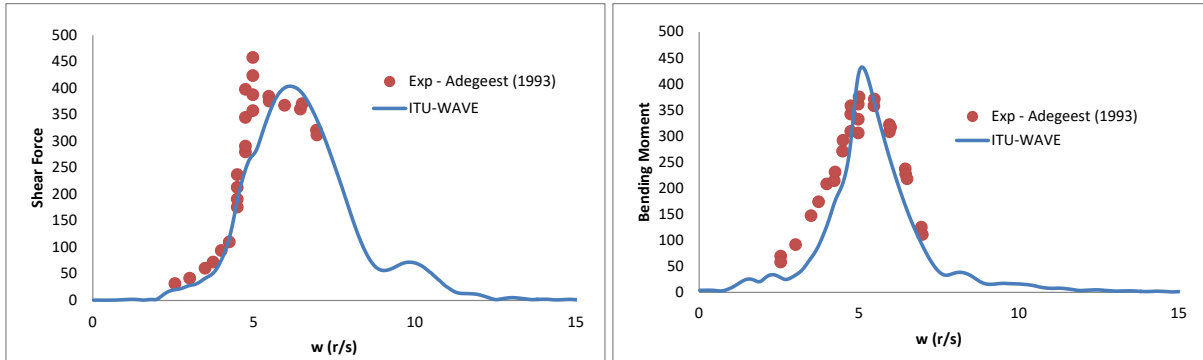

Fig. 17: Wigley I hull shear force and bending moment at Fn = 0.2 and $\beta = 180^0$ – potential approach

It can be seen from Fig. 17 that ITU-WAVE numerical results has satisfactory agreement with experiment results (Adegeest 1994). Shear force and bending moment using 8 free-free beam modes are obtained by the first and second integration of Eq. (21), respectively after the force coefficients $F_j(\omega)$ are determined by the use of Eq. (22).

10. Wave energy converters (WEC) with latching control

Latching control, which is a discrete real time control, is used in the present paper. Rather than adapting WEC parameters to the excitation force in order to optimize the linear body response, the latching control adapts the body response to WEC and to the excitation in a nonlinear fashion. It is a kind of parametric resonance adaptation process as can be found in nonlinear oscillatory theory, this kind of behaviour can be predicted only using time domain simulations. Latching control can magnify the amplitude of the motion

whatever the frequency of the excitation force, and can improve the efficiency of WEC in terms of absorbed energy for excitation frequencies apart from the natural frequency.

When latching control is applied, an additional force must be introduced in the dynamic of WEC to cancel the acceleration of the controlled motion in order to lock the system temporarily. The latching control of WEC consists of locking the oscillating body in position at the instant when velocity vanishes, and releasing it after a certain delay to be determined. This latching delay has to be applied in order to maximise the response amplitude of the body. The instant of latching is imposed by the dynamics of the body itself (*i.e.* vanishing velocity); thus the control variable is simply the duration of the latching phase, or equivalently the instant of release (Greenhow *et.al.* 1997, Eidsmoen 1998, Babarit *et.al.* 2004, Kara 2010). One of the advantages of latching control is that it is passive, which means that it does not need to deliver energy to WEC while it is engaged, since the forces do no work as long as the velocity vanishes.

10.1. Instantaneous and mean absorbed power

The instantaneous power $P_{ins_k}(t)$ absorbed by Power-Take-Off (PTO) system for each mode is directly proportional to exciting force (which is the sum of diffraction and Froude-Krylov forces) and radiation forces on floating bodies and is defined as (Kara 2016)

$$P_{ins_k}(t) = [F_{exc_k}(t) + F_{rad_k}(t)]\dot{x}_k(t) \qquad (23)$$

Where k represents each mode of motion (e.g. heave), $F_{exc_k}(t)$ exciting forces which are due to incident and diffracted waves, $F_{rad_k}(t)$ radiation forces which are due to the oscillation of bodies.

$$F_{exc_k}(t) = F_k(t) = \int_{-\infty}^{\infty} d\tau K_{kD}(t-\tau)\zeta(\tau) \quad (24)$$

$$F_{rad_k}(t) = F_{kk}(t) = -a_{kk}\ddot{x}_k(t) - b_{kk}\dot{x}_k(t) - c_{kk}x_k(t) - \int_0^t d\tau K_{kk}(t-\tau)\dot{x}_k(\tau) \quad (25)$$

The power due to exciting forces $P_{exc_k}(t) = F_{exc_k}(t)\dot{x}_k(t)$ is the total absorbed power from the incident and diffracted waves, whilst the power due to radiation forces $P_{rad_k}(t) = F_{rad_k}(t)\dot{x}_k(t)$ is the power radiated back to sea due to the oscillation of floating body. The mean (average) power $\overline{P_{ins_k}(t)}$ absorbed by the PTO system over a time range T is given as

$$\overline{P_{ins_k}(t)} = \frac{1}{T}\int_0^T dt[F_{exc_k}(t) + F_{rad_k}(t)]\dot{x}_k(t) \quad (26)$$

The averaging time T must be much larger than the characteristics period of the incident wave which is approximately from 5s to 15s. In order to avoid the transient effects, only the last half of the time domain results are taken into account for the prediction of the mean absorbed power using Eq. (26) and other time dependent parameters in ITU-WAVE numerical code.
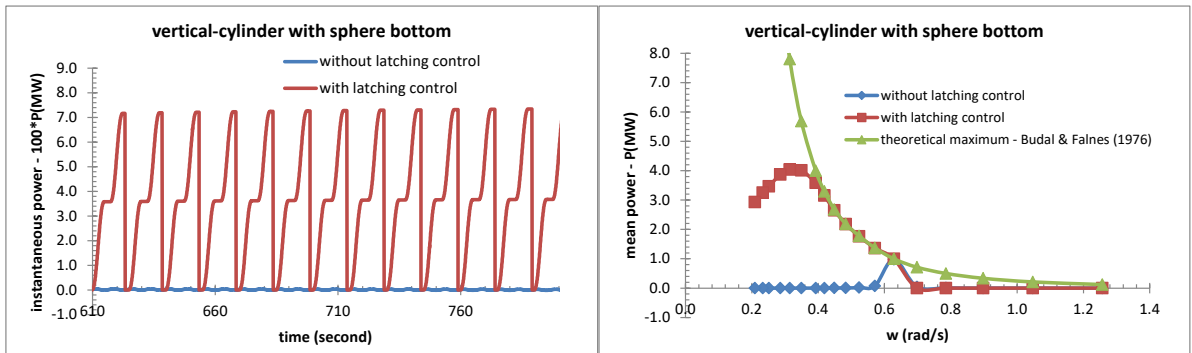
Fig. 18: Instantaneous power (left) absorbed by a vertical-cylinder with sphere bottom at each period with and without latching control at resonance period at 10s and incident wave period at 15s with 1m wave amplitude, absorbed mean power (right) with and without latching control in the range of frequencies – potential approach

Fig. 18 shows the instantaneous power (left) absorbed for incident wave period of 15s from ocean waves using a vertical-cylinder with sphere bottom (which has 8m radius and 13m draft and free to heave mode and fixed for other modes) as a wave energy converter with and without latching control. In the case of latching control the absorbed instantaneous power is increased significantly. It may be noticed that the unlatching results are very small in terms of controlled latching results. Fig. 18 shows also the absorbed mean power (right) for the range of incident wave frequencies. In the case of latching control the absorbed mean power is again increased significantly. The theoretical maximum power $P = \rho g^3 \zeta_a/(4\omega^3)$ in regular seas (Budal and Falnes 1976) is compared with ITU-WAVE numerical results. As can be seen from Fig. 18 (left) the absorbed mean power at low frequencies which has more power compared to high frequencies are increased significantly with latching control.

10.2. Efficiency

The efficiency η of WECs is defined as $\eta = l/l_{max}$ which has a maximum of 1.0 for any wavelength. The capture width l and maximum capture width l_{max} is defined as (Budal and Falnes 1976) $l = \bar{P}_{ins_k}/P_w$ and $l_{max} = \lambda/(2\pi)$ where $\bar{P}_{ins_k}(t)$ is the mean power and given by Eq. (26), $P_w = \rho g^2 \zeta_a^2/(4\omega)$ is the wave power in the incident wave train per unit crest length, ζ_a being the incident wave amplitude. A good wave absorber is a body which has the ability when making waves, to concentrate the wave energy along a narrow sector rather than distribute the energy evenly over all angles. The maximum capture width equals to $l_{max} = \lambda/(2\pi)$ for an axisymmetric system in symmetric mode of motion e.g. heave. This implies that the floating body absorbs all the power in an incident wave equal to that passing a crest length of $\lambda/(2\pi)$.
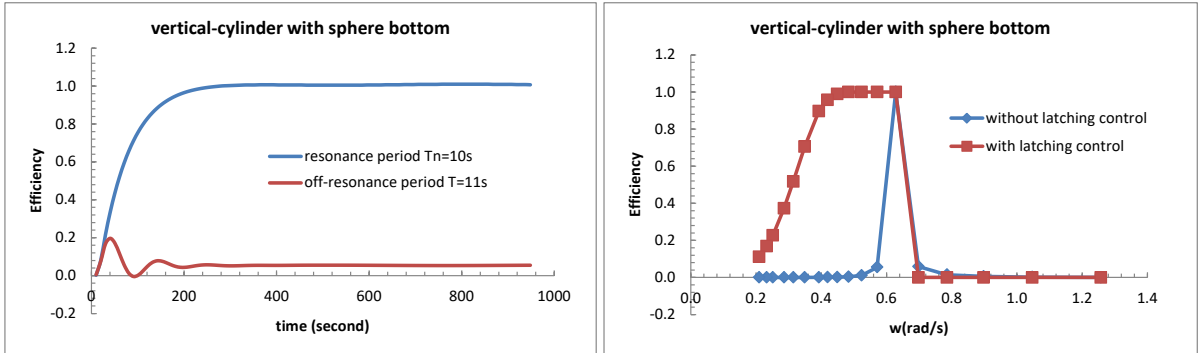

Fig. 19: Convergence of efficiency for resonance and off-resonance period without latching control for a vertical-cylinder with sphere bottom (left) and efficiency with and without latching control at a range of frequencies (right) – potential approach

Fig. 19 (left) shows the efficiencies for vertical-cylinder with sphere bottom in the case of in resonance and off-resonance periods. The efficiency converges to 1.0 (100% efficient) at resonance period $T_n = 10s$ whereas off-resonance case $T = 11s$ shows a very low efficiency (5%). Figure 19 (right) shows the efficiency plotted at a range of frequencies. If the natural period of vertical-cylinder equals the period of incident waves in the case of without latching control, the device is perfectly tuned and we expect optimal efficiency. As the difference between natural period of device and incident wave period increases, the efficiency of the system decreases. As can be seen in Figure 19(right) latching control increases the bandwidth of the wave energy converter for lower frequency ranges. If off-resonance period is 11s (0.571 rad/s), the efficiency is approximately 5% without latching control. However, if $1s$ latching is applied, it is possible to achieve an efficiency of approximately 100%.

11. Conclusions

The application of a three-dimensional transient wave-body interaction computer numerical code ITU-WAVE with Boundary-Integral Equation Method (BIEM) and Neumann-Kelvin linearization was presented

for the time domain prediction of different hydrodynamic parameters including the first order motions and the first-order unsteady hydrodynamic forces e.g. the radiation, exciting forces of the mono-hull and multi-hull floating bodies, the first and second order steady forces, multi-body interactions, hydroelastic analysis, power absorptions from ocean waves, wave energy converter arrays.

As the equation of motion requires long time simulation in order to achieve steady state condition and the first order steady problem is solved as the steady state limit of the radiation problem, this implies that the transient free-surface Green function must be evaluated a large number of times to reach steady state limits. This numerical process is too expensive for practical purposes. To avoid expensive transient free-surface Green function calculations, the asymptotic continuation of the impulse response function of the first order unsteady problem and the wave-resistance, sinkage force, and trim moment of the first order steady problem is studied using the Least Square fitting to reduce the computational time.

It was shown that the behaviour of both two and four truncated vertical cylinder arrays results is significantly different from those of mono-hull due to trapped waves in the gap of arrays. It was also shown numerically the hydrodynamics interactions are effective in the whole frequency range and are even stronger in a limited frequency range which is of interest for floating body motions in waves.

The prediction of the added-resistance of the floating bodies (which is the longitudinal component of the mean second order wave forces in the case of non-zero forward speed and can be computed from quadratic product of the first-order quantities) is presented using the near-field method based on the direct pressure integration over floating body in time domain. The numerical experience shows that the biggest contribution due to radiation problem to the added resistance will be in the region of the resonance frequency of heave and pitch motions. The diffraction induced added resistance will be dominated by high incident wave frequencies where the floating body motions are small.

A non-dimensional structural stiffness parameter $S = EI/\rho g L^5$ is used and depending on this stiffness parameter the hydroelatic effects of floating slender barge are studied for RAOs. A Wigley I hull form is then studied as a stiff structure in order to determine the effects of elastic modes due to rigid body modes only which are coupled with elastic modes. The effects of the different incident wave lengths and geometry of floating bodies are taken into account for the prediction of bending moment and shear force.

The numerical results show that the efficiency of WEC is considerably improved by the latching control which enlarges the bandwidth of WEC in the low frequencies, if the exciting force is predicted in the close future of the unlatching time and that body is hold in position during the latching time. The numerical experience also showed that the decision to release or not WEC at a current time depends on the future of the system beyond the current time. The better this quantity can be predicted, the closer the converted power may approach the theoretical maximum.

The numerical results were also presented to demonstrate the convergence of the developed computer code ITU-WAVE for the IRFs, added-mass and damping coefficients, exciting forces, RAOs, the first-order steady forces (e.g. wave resistance, sinkage force, and trim moment), the second-order mean drift forces (e.g. added resistance), shear force, bending moment, and efficiency of wave energy converters. ITU-WAVE computational numerical results are shown to be in satisfactory agreement with analytical, other numerical and experimental results.

References

Adachi H, Ohmatsu S, 1979. On the influence of irregular frequencies in the integral equation solution to the time-dependent free surface problems. Journal of Society of Naval Architect of Japan, 146, 127-135.

Adegeest L., 1994. Experimental investigation of the influence of bow flare and forward speed on the nonlinear vertical motions, bending moments and shear forces in extreme regular wave conditions.

Laboratory of Ship Hydromechanics, Delft University of Technology, Report Nr. 993, The Netherlands.

Babarit A, Duclos G, Clement AH., 2004. Comparison of latching control strategies for a heaving wave energy device in random sea. Applied Ocean Research, 26, 227-238

Baker G.R., Meiron D.I., Orszag S.A., 1982. A Generalized Vortex Methods for Free Surface Flow Problem *Journal of Fluid Mechanic* **123**, 477-501.

Beck RF, Liapis S, 1987. Transient Motions of Floating Bodies at Zero Forward Speed. Journal of Ship Research, 31(3), 164-176.

Beck R.F. and Magee A.R., 1991. Time Domain Analysis for Predicting Ship Motions. *Proceedings of the IUTAM Symposium on the Dynamics of Marine Vehicles and Structures in Waves, Brunel University, 49-64*.

Beck R.F., 1999. Fully Nonlinear Water Wave Computations Using a Desingularized Euler-Lagrange Time Domain Approach. In *Nonlinear Water Wave Interaction*, 1-57.

Bertram V, 1990. Ship Motions by Rankine Source Method. Ship Technology Research, 37 (4), 143-152.

Bingham H.B., Korsmeyer, F.T., Newman J.N., 1994. Prediction of Seakeeping Charecreristics of Ships. Proceedings of the 20th Symposium on Naval Hydrodynamics, Santa Barbara, California, C.A., 19-38.

Budal K, Falnes J., 1976. Optimum operation of wave power converter. Internal Report, Norwegian University of Science and Technology

Cummins WE, 1962. The Impulse Response Function and Ship Motions. Shiffstechnik, 9, 101-109.

Danmeier DG., 1999. A higher-order panel method for large-amplitude simulations of bodies in waves. PhD Thesis, MIT.

Eidsmoen H., 1998. Tight-moored amplitude limited heaving buoy wave energy converter with phase control. Applied Ocean Research, 20, 157-161.

Faltinsen O., 1977. Numerical Solution of Transient Nonlinear Free Surface Motion Outside or Inside Moving Bodies. In *Proceedings of the 2nd International Conference on Numerical Ship Hydrodynamics, Berkeley, California, C.A.,* 347-357.

Ferrant P., 1990. A Coupled Time and Frequency Approach for Nonlinear Wave Radiation. In *Proceedings of the 18th Symposium on Naval Hydrodynamics, Ann Arbor, Michigan,* 67-84.

Finkelstein A.B., 1957. The Initial Value Problem for Transient Water Waves. *Communications on Pure and Applied Mathematics.***10***,* 511-522*.*

Greenhow M, White SP., 1887. Optimal heave motion of some axisymmetric wave energy devices in sinusoidal waves. Applied Ocean Research, 19, 141-159

Hess J.L., Smith A.M.O., 1964. Calculation of Non-Lifting Potential Flow about Arbitrary Three-Dimensional Bodies. *Journal of Ship Research* **8***,* 22-44*.*

Hulme A, 1982. The Wave Forces Acting on a Floating Hemisphere Undergoing Forced Periodic Oscillations. Journal of Fluid Mechanic, 121, 443-463.

Inoue Y, Kamruzzaman M, 2008. Analysis of hydrodynamic characteristics for arbitrary multihull ships advancing in waves. Journal of Marine Science and Technology, 13, 231-243.

Journee J.M.J., 1992. Experiment and Calculations on Four Wigley Hullforms. *Report No. 909*, Delft University of Technology Ship Hydrodynamics Laboratory.

Kagemoto H, Yue DKP., 1986. Interactions among multiple three-dimensional bodies in water waves: an exact algebraic method. Journal of Fluid Mechanics, 166, 189-209.

Kara F., 2000, Time domain hydrodynamics and hydroelastics analysis of floating bodies with forward speed. PhD thesis, University of Strathclyde, UK

Kara F, Vassalos D., 2003. Time domain prediction of steady and unsteady marine hydrodynamic problem. *International Shipbuilding Progress,* 50(4), 317-332.

Kara F, Vassalos D., 2005. Time domain computation of wavemaking resistance of ships. Journal of Ship Research, 49 (2), 144-158.

Kara F, Vassalos D., 2007. Hydroelastic analysis of cantilever plate in time domain. Ocean Engineering, 34, 122-132.

Kara F., 2010. Time domain prediction of power absorption from ocean waves with latching control. Renewable Energy, 35, 423-434.

Kara F., 2011. Time domain prediction of added-resistance of ships. Journal of Ship Research, 55 (3), 163-184.

Kara F., 2015. Time domain prediction of hydroelasticity of floating bodies. Applied Ocean Research, 51, 1-13.

Kara F., 2016. Time domain prediction of seakeeping behaviour of catamarans. International Shipbuilding Progress, 62 (3-4), 161-187.

Kara F., 2016. Time domain prediction of power absorption from ocean waves with wave energy converter arrays. Renewable Energy, 92, 30-46.

Kara F, 2016. Point absorber wave energy converter in regular and irregular waves with time domain analysis. International Journal of Marine Science and Ocean Technology, 3(7), 74-85.

Kara F, 2017. Control of wave energy converters for maximum power absorptions with time domain analysis. Journal of Fundamentals of Renewable Energy and Applications, 7(1), 1-8

Kim, C.H., Chou, F.S., Tien, D., 1980. Motion and Hydrodynamic Loads of a Ship Advancing in Oblique Waves. Transactions of the Society of Naval Architects and Marine Engineers **88**, 225-256.

King, B., 1987. Time Domain Analysis of Wave Exciting Forces on Ships and Bodies. PhD Thesis. Department of Naval Architecture and Marine Engineering, University of Michigan.

Korvin-Kroukovsky B.V., Jacobs W.R., 1957. Pitching and Heaving Motions of a Ship in Regular Waves. Transaction of the Society of Naval Architects and Marine Engineers, **65**, 590-632.

Kring D, Sclavounos PD, 1991. A New Method for Analyzing the Seakeeping of Multi-Hull Ships. Proceedings of 1st International Conference on Fast Sea Transportation, Trondheim, Norway, 429-444.

Lee C-H, Newman J.N., 2000. An assessment of hydroelasticity for very large hinged vessels. Journal of Fluid and Structures, 14, 957-970.

Liapis, S., Beck, R.F., 1985. Seakeeping Computations Using Time Domain Analysis. In Proceedings of the 4th International Symposium on Numerical Hydrodynamics, Washington, D.C., 34-54.

Liapis, S., 1986. Time Domain Analysis of Ship Motions. PhD Thesis. Department of Naval Architecture and Marine Engineering, University of Michigan.

Lin, W.C., Yue, D.K.P., 1990. Numerical Solutions for Large Amplitude Ship Motions in the Time Domain. In Proceedings of the 18th Symposium on Naval Hydrodynamics, Ann Arbor, Michigan, 41-66.

Longuet-Higgins M.S., Cokelet E.D., 1976. The Deformation of Steep Surface Waves on Water- A Numerical Method of Computation. *Proceedings of the Royal Society of London, Series A,* **350***,* 1-26.

Malenica S, Molin B, Remy F, Senjanovic I., 2003. Hydroelastic response of a barge to impulsive and non-impulsive wave loads. Hydroelasticity in Marine Technology, Oxford, UK, 107-115.

McCarthy JH, 1979. Overview of Results. Proceedings of the Workshop on Ship Wave Resistance Computations, Bethesda, Maryland.

Nakos D, Sclavounos PD, 1990. Ship Motions by a Three Dimensional Rankine Panel Method. Proceedings of the 18th Symposium on Naval Hydrodynamics, Ann Arbor, Michigan, USA, 21-41.

Newman J.N., 1985. Transient Axisymmetric Motion of a Floating Cylinder. *Journal of Fluid Mechanic, 157, 17-33*

Newman J.N., 2005. Efficient hydrodynamic analysis of very large floating structures. Marine Structures, 18, 169-180.

Noblesse F, 1983. Summary of the cooperative experiment on Wigley parabolic model in Japan. Proceedings of the second Workshop on Ship Wave Resistance Computations, Bethesda, Maryland.

Ogilvie TF, 1964. Recent Progress toward the Understanding and Prediction of Ship Motions. Proceedings of the 5th Symposium on Naval Hydrodynamics, Office of Naval Research, Washington, D.C., USA, 3-128.

Ogilvie, T.F., Tuck, E.O., 1969. A Rational Strip Theory for Ship Motions, Part 1. Report No. 013, The Department of Naval Architecture and Marine Engineering, The University of Michigan, Ann Arbor, Michigan.

Ohkusu M., 1969. On the heaving motion of two circular cylinders on the surface of a fluid. Reports of Research Institute for Applied Mechanics, No. 58, 17, 167-185

Salvensen, N., Tuck, E.O., Faltinsen, O., 1970. Ship Motions and Sea Loads. Transactions of the Society of Naval Architects and Marine Engineers **78**, 250-287.

van Oortmerssen G., 1979. Hydrodynamic interaction between two structures floating in waves. Proceedings of the 2nd International Conference on Behaviour of Offshore Structures (BOSS'79), London, UK, 339-356.

Vinje T., Brevig P., 1981. Nonlinear Ship Motions. In *Proceedings of the 3rd International Symposium on Numerical Hydrodynamics,* 257-268.

Xiang X, Faltinsen OM, 2011. Time domain simulation of two interacting ships advancing parallel in waves. Proceedings of the ASME 30th International Conference on Ocean, Offshore and Arctic Engineering, Rotherdam, The Netherlands.

Yuan Z-M, Incecik A, Day A, 2014. Verification of a new radiation condition for two ships advancing in waves. Applied Ocean Research, 48, 186-201.

Wehausen J.V., Laitone E.V., 1960. Surface Waves. *Handbuch der Physik* **9***,* 446-778.

Wehausen J.V., 1964. Effect of the Initial Acceleration upon the Wave Resistance of Ship Models. Journal of Ship Research, **7***,* 38-50.